

# Flux Intensifying PM-Motor with Variable Leakage Magnetic Flux Technique

Masahiro Aoyama<sup>1\*</sup> and Toshihiko Noguchi<sup>2</sup>

<sup>1</sup> Electric Component Development Department, SUZUKI Motor Corporation, Hamamatsu, JAPAN

<sup>2</sup> Graduate School of Science and Technology, Shizuoka University, Hamamatsu, JAPAN

\*E-mail: aoyamam@hhq.suzuki.co.jp

**Abstract**— This paper describes a flux intensifying PM-motor with variable magnetic flux. The unique feature of this proposed motor is the ability to passively adjust the magnetic flux linkage into the armature windings in proportion to the armature magnetomotive force and/or armature current phase. The magnetic circuit topology of the flux intensifying PM-motor and the passive variable leakage magnetic flux are determined through FE-analysis. Then, the driving performance is experimentally elucidated through comparison with that of a reverse pole type (flux weakening) PM-motor without variable leakage magnetic flux.

**Keywords**— Permanent magnet type synchronous motor, variable leakage magnetic flux, flux intensifying.

## I. INTRODUCTION

Recently, strengthening of global environmental regulations, are accelerating the EVs (Electric Vehicles) development for the zero-emission society in the transportation equipment sector. In general, as traction motor for EVs, an IM (Induction Machine) and a PMSM (Permanent Magnet Synchronous Motor) is employed mainly [1-4]. These motors are selected as the suitable motor by a target and the common use drive domain of the vehicle. In the case of PMSM, high torque density can be realized, and high efficiency drive can be realized in the range of low-load to maximum load while low-speed and medium-speed range. On the other hand, in the extremely low-speed range, the efficiency is lower than IM due to the iron loss caused by the magnetic flux of the PMs (Permanent Magnets). At higher loads in the high speed range, iron loss increases due to large distortion of the gap magnetic flux which is caused by flux weakening control, resulting in lower efficiency than IM.

In view point of the above problems, studies on variable magnetic flux motors have been actively studied in recent years for the purpose of expanding the PMSM's high efficiency area and output. As representative studies of today, 1) the memory motor type that makes the PM flux of the PMSM variable [5-8], 2) the type to adjust the rotor skew angle [9], 3) the type to adjust the iron-pole magnetization amount of the consequent pole structure [10-13], and 4) the type that utilizes the leakage magnetic flux [14-18]. Particularly in the case of 4), the variable magnetic flux function is realized only by devising the

magnetic circuit design of the rotor while applying the conventional vector control as it is without requiring the variable-magnetized magnets and extra additional devices. It has a simple structure that passively controls the short magnetic flux path in the rotor by the armature magnetomotive force and the armature magnetic flux vector which is greatly different from the conventional variable magnetic flux technique. This technique is superior in terms of cost, control, and robustness. However, there is a problem in Ref. [14] and [15], that is difficult to utilize the reluctance torque because the variable magnetic flux range is narrow and the leakage magnetic flux amount tends to increase as the armature current vector advances. On the other hand, in Ref. [16] and [17], since the PMs are arranged in the salient pole portions, the salient pole ratio is low, which is a factor of lowering the torque density.

In view point of the above problems of the prior studies, the authors have been studied the possibility of a passive variable magnetic flux range and improve the reluctance torque by combining field adjustment by variable leakage magnetic flux and flux intensifying effect by the  $+d$ -axis armature magnetic flux [19],[20]. The following three points differ from the prior studies,

A) Study of possibility of utilization of reluctance torque by designing the forward saliency circuit which attempted to improve the forward saliency ratio by separating the iron core magnetic path and the PM-magnetic path.

B) A magnetic circuit design in which the leakage magnetic flux path of PM-flux is formed in an iron core magnetic path provided between PM-magnetic paths by applying the concept of a consequent pole structure. The leakage magnetic flux is induced by the magnetic shielding effect on the magnetic flux on the magnet by the  $q$ -axis armature magnetic flux.

C) Place the salient pole on the  $d$ -axis and alternately arrange the PM-magnetic path and the iron core magnetic path between the  $d$ -axis and the  $q$ -axis. Under the flux intensifying control, i.e.,  $+d$ -axis armature magnetic flux is so arranged as to face the same direction, the  $d$ -axis armature magnetic flux of the iron core magnetic path becomes the forward direction with respect to the PM-magnetic flux and performs flux intensifying. The

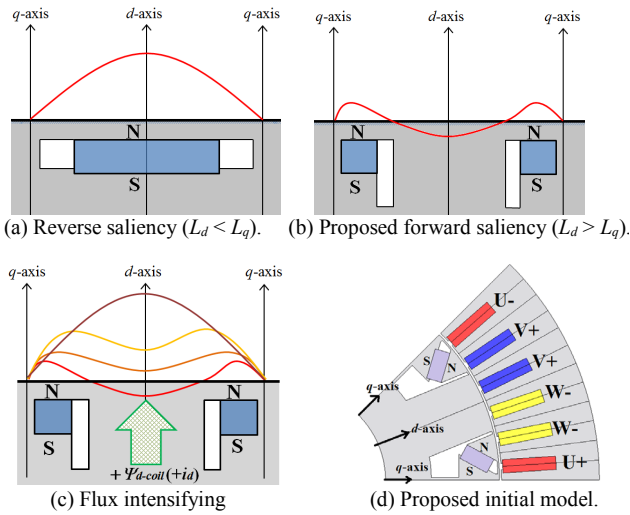


Fig. 1. Concept of proposed flux intensifying PM-motor.

amount of flux intensifying becomes variable according to the  $d$ -axis armature magnetic flux.

In this paper, the concept of magnetic circuit design for achieving the variable magnetic flux principle having the above characteristics is described. Then, the prototype for principle verification and comparing the drive performance with that of the reverse salient pole type PM-motor of the same core size without variable leakage magnetic flux function is experimentally demonstrated. In addition, verification of the possibility of the proposed variable magnetic flux PM-motor, drive characteristics, and problems will be elucidated.

## II. PRINCIPLE OF PROPOSED VARIABLE MAGNETIC FLUX

Generally, as shown in Fig. 1 (a), PM magnetomotive force is designed so that magnetic flux is distributed sinusoidally, but the proposed motor is intentionally designed such that a iron core is provided between the magnets and the waveforms with superimposing the positive third harmonic as shown in Fig. 1 (b). On the other hand, under the load condition, the third harmonic wave superimposed on the PM-magnetic flux is canceled by the  $+d$ -axis armature magnetic flux, and the combined magnetic flux of the PM-flux and the armature magnetic flux is distributed in the sinusoidal wave as shown in Fig. 1 (c). Applying this concept, it is possible to reduce the no-load core loss under no-load, reduce the iron loss due to the PM-flux at the time of extremely low load, and adjust the amount of flux intensifying by adjusting the  $+d$ -axis armature magnetic flux amount as the load increases. In the prior research of Refs. [14-17], flux bypass magnetic path are provided on both sides of magnets arranged on the  $d$ -axis to passively change armature flux linkage amount by armature magnetomotive force and current vector. Although the leakage magnetic flux of the proposed motor also the same with conventional technique, however, applying the concept of the consequent pole structure as shown in Fig. 2, the iron core magnetic flux path between PM-flux path, the leakage magnetic flux formed by the iron core

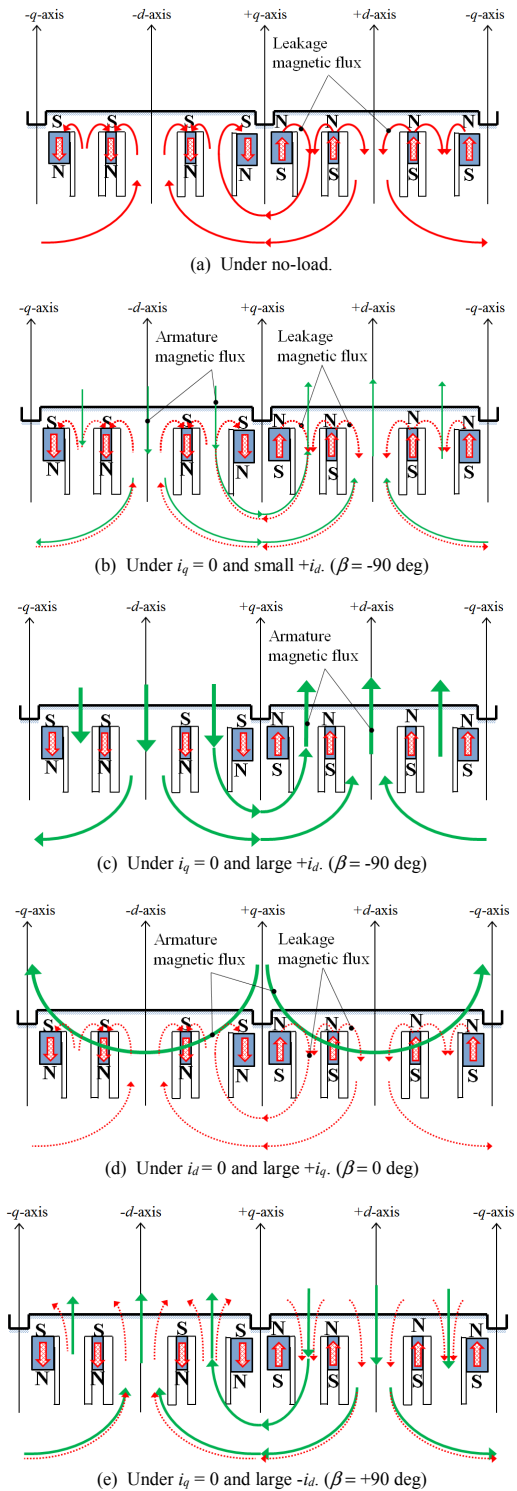


Fig. 2. Leakage PM-flux and armature magnetic flux with respect to armature magnetomotive force and armature current vector.

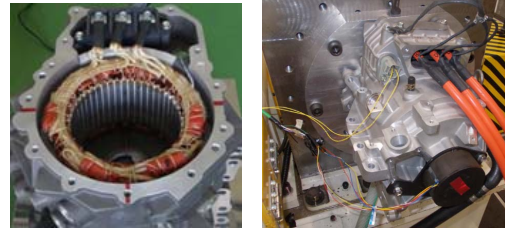
magnetic flux path is variable with the  $+d$ -axis armature magnetic flux amount and the armature current vector. As a result, the change of the armature interlinkage flux number is passively increased by the armature magnetomotive force and the current vector. On the other hand, the iron core magnetic flux path becomes a magnetic path of the armature magnetic flux and contributes to the generation of the reluctance torque.

Table I. Specifications of prototype.

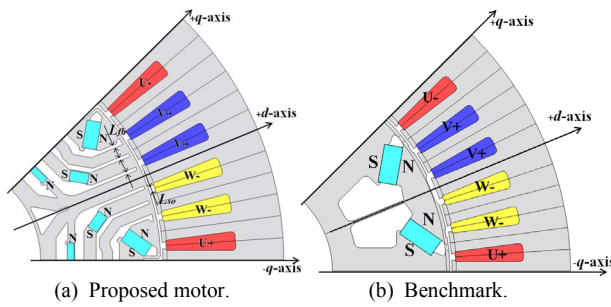
	Benchmark	Proposed
Number of rotor poles	8	
Number of stator slots	48	
Stator core outer diameter	200 mm	
Air-gap length	0.7 mm	
Axial length of core	108 mm	
Maximum armature magnetomotiveforce	1060 A <sub>rms</sub> T (28.1 A <sub>rms</sub> /mm <sup>2</sup> ), 60 s	
Number of armature coil-turn	12	
Armature winding connection	2 series-4 parallel	
Armature winding resistance	12.76 mΩ/phase	
Core material	35H-EA (Nippon steel & Sumitomo metal)	
Magnet material	N39UH (Shinetsu chemical)	N52AS-GF (Shinetsu chemical)



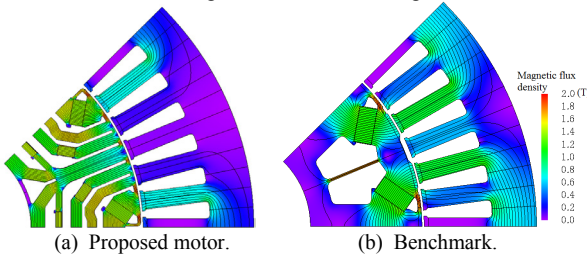
(a) Rotor core of proposed (b) Rotor core of benchmark and stator core.



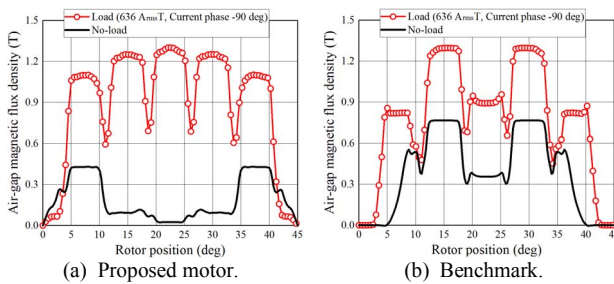
(c) Stator assembly (Left-side) and experimental setup (Right-side).  
Fig. 6. Actual prototype.



(a) Proposed motor. (b) Benchmark.  
Fig. 3. Cross section diagram.



(a) Proposed motor. (b) Benchmark.  
Fig. 4. Magnetic flux lines under no-load.



(a) Proposed motor. (b) Benchmark.  
Fig. 5. Air-gap magnetic flux waveforms.

### III. PROTOTYPE MACHINE

Magnetic circuit and structural design of the proposed principle verification machine were performed with the specifications in Table I. The advantages of proposed motor will be revealed with comparing that of benchmark model. The benchmark and the proposed motor are designed with a common stator, the same air-gap length, the same magnet volume, the same core material and the same core stack length. For the magnet, a magnet suitable for the necessary coercive force is selected from the

difference of the magnetic circuits of both motors, respectively. Figure 3 shows the cross section diagram of magnetic circuit design of proposed motor and benchmark. Figure 4 shows the magnetic flux density and flux lines under no-load and Fig. 5 shows the magnetic flux density waveform in air-gap (intermediate position between stator and rotor) under no-load (black solid line) and load with  $+d$ -axis armature current (red dotted line). As can be seen in these figures, the proposed motor leaks PM-flux into the iron core magnetic flux path on the  $d$ -axis (rotor position 22.5 deg is  $+d$ -axis) and a short-circuited magnetic path is formed inside the rotor. On the other hand, in the benchmark, the magnetic resistance of the both end bridges on the outside of the magnetic pole and the  $d$ -axis center bridge is higher than the magnetic resistance of the air-gap, so the larger number of PM-fluxes are linked to the stator than the proposed motor. Next, when comparing the air-gap magnetic flux density waveform at the flux intensifying state (current phase  $-90$  deg) due to the  $+d$ -axis armature magnetic flux in Fig. 5, it can be confirmed that the slot harmonic is superimposed on the proposed motor, but it is possible to obtain a sinusoidal gap magnetic flux waveform. In the current phase, the  $+q$ -axis is the phase reference and the CCW direction is positive. Here, in order to facilitate the formation of a short-circuit magnetic flux in the rotor according to the condition of the armature magnetomotive force and the current phase, the width of the flux barrier ( $L_{fb}$  in the Fig. 3 (a)) separating the iron core magnetic flux path and the PM-flux path from the slot open width ( $L_{so}$  in the Fig. 3 (a)) of the stator is designed narrow. That is, the magnetic circuit is designed so that the magnetic resistance of the leakage flux magnetic path becomes small when the armature magnetic flux is perpendicular to the PM-flux.

Figure 6 shows the prototype of the benchmark and the proposed motor. Both motors has the distributed winding stator structures with 8 poles-48 slots (number of phase slots per pole  $q = 2$ ), and the armature winding adopts AW round wire with H-type heat resistant class. Both rotors are not skewing. Peripheral parts such as shaft and end-plate of both rotors are prototyped with

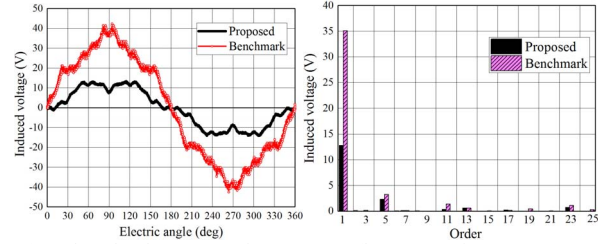
common parts. The stator is attached to a water-cooled motor case by shrink fitting. Performance evaluation of both motors is performed by replacing the rotor of Fig. 6 (a) and (b) and assembling.

IV. EXPERIMENTAL TEST

A. Current Phase-vs.-Torque Characteristics

A universal inverter manufactured by Myway Plus Inc. was used to motor drive and set the carrier frequency to 8 kHz. The torque measurement was carried out with speed control on the motor bench side and torque control with the inverter for driving the test motor. It is controlled by sinusoidal wave PWM driving, the DC-bus voltage is set at  $245\text{-}V_{dc}$ , and the upper limit of the voltage utilization rate with respect to DC-bus voltage is set within the range of 95-96 %. Figure 7 shows the no-load induced voltage waveform at 1000 r/min and its harmonic analysis results. According to the figure, magnets with the same volume per pole and high residual magnetic flux density  $B_r$  are adopted from Table I, but as shown in Fig. 2, the proposed motor is short-circuited with the PM flux in the rotor at no-load, the armature interlinkage magnetic flux number decreases, and as a result, the induced voltage becomes extremely lower than the benchmark.

Figure 8 shows the current phase-vs.-torque characteristics of the benchmark and the proposed motor. The  $+q$ -axis is defined as the current phase reference and the  $-d$ -axis direction is defined as the advanced angle direction. In measurement of the reluctance torque in the figure, measurement is made using unmagnetized magnets. For the convenience of the measurement bench, measurement was made with a load of 70 % of design value as the upper limit. Comparing the reluctance torques of both motors, under the armature magnetomotive force  $750\text{ A}_{rms}\text{T}$ , the proposed motor stays as only 66.3 % of the benchmark. In the total torque, the proposed motor is only about 59.2 % of the benchmark. It can be cited whether or not the armature reaction torque can be used as a main cause that the forward salient pole PM-motor is much lower in torque density than the reverse salient pole PM-motor. As shown in Fig. 9, in the case of the forward salient pole type PM-motor, it is necessary to drive the flux intensifying with saliency of  $L_d > L_q$ . It is necessary to design the magnetic circuit so that the  $dq$ -axis magnetic path does not interfere around the MTPA point. Meanwhile, since the reverse salient pole type PM-motor is driven by flux weakening, a permanent magnet having sufficient coercive force is arranged on the  $d$ -axis to have reverse saliency of  $L_d < L_q$ , the armature reaction torque can be utilized. As a result, the torque generation surface of proposed motor is enlarged more than the forward salient pole type PM-motor, realizing high torque density. In the case of flux intensifying PM-motor, it is necessary to design the magnetic circuit so that the  $dq$ -axis magnetic path does not interfere. Therefore, if the same volume of magnet is embedded in the rotor of the same core size, the core magnetic path inevitably narrows in width and becomes easy to be magnetically saturated, so that the



(a) Induced voltage waveforms. (b) Harmonic contents. Fig. 7. Induced voltage waveforms and its harmonic contents.

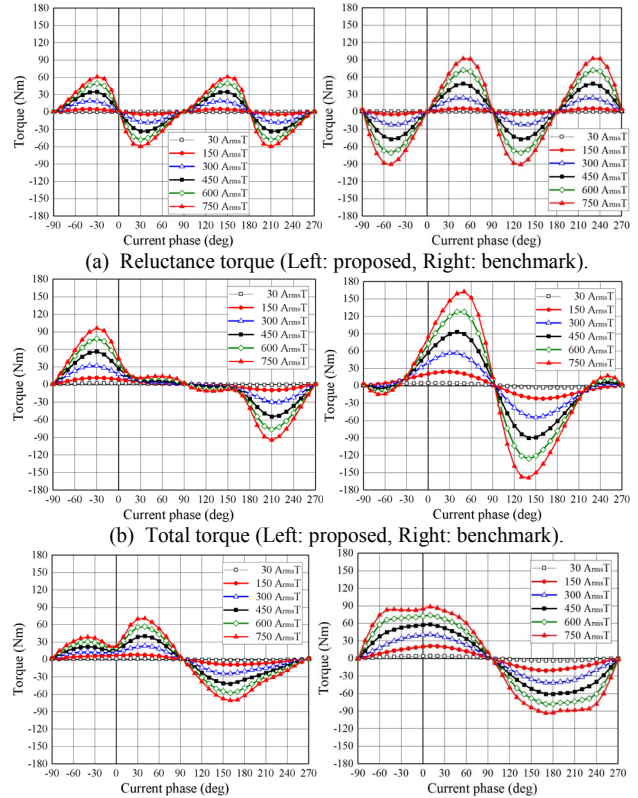


Fig. 8. Current phase-vs.-torque characteristics.

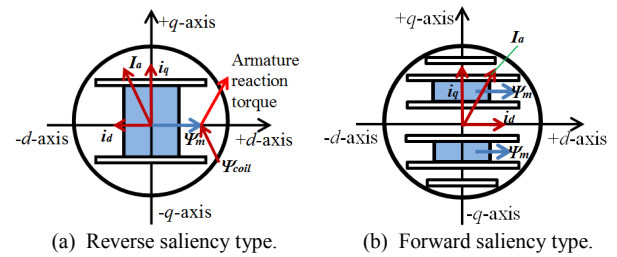


Fig. 9. Simplified rotor model.

reluctance torque of the forward salient pole PM-motor is inferior to that of the reverse salient pole PM-motor.

Next, in order to confirm the passive variable magnetic flux effect of the proposed motor, the magnet torque was approximated by the difference between the total torque and the reluctance torque shown in Fig. 8 (a) and (b). Figure 8 (c) shows the current phase-vs.-magnet torque characteristics. From this figure, the magnet torque of the benchmark is the theoretical  $\cos\beta$ -function, but it can be confirmed that the magnet torque of the proposed motor drops greatly when the current phase is

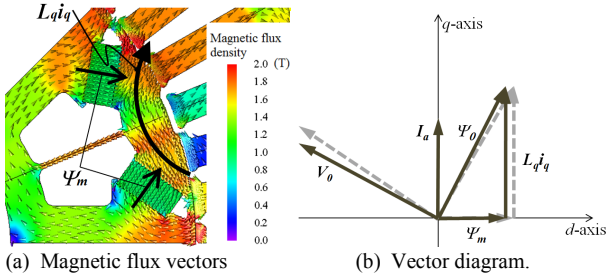


Fig. 10. Magnetic flux vectors and vector diagram under high-load and current phase 0 deg. (Benchmark).

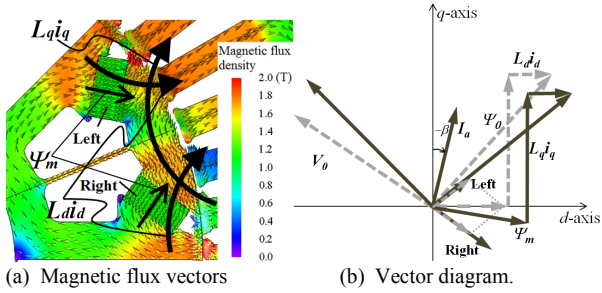


Fig. 11. Magnetic flux vectors and vector diagram under high-load and current phase -30 deg. (Benchmark).

near 0 deg. As described in the previous chapter, when  $\beta = 0$  deg, the flux intensifying effect does not effects due to the  $+d$ -axis armature magnetic flux  $\Psi_{+d-coil}$  becomes zero. As a result, the leakage magnetic flux linking to the iron core magnetic flux path increased and the magnetic flux linking the stator decreased as shown in Fig. 2 (d). Furthermore, the  $+q$ -axis armature magnetic flux  $\Psi_{+q-coil}$  is orthogonal to the magnetic flux vector. The larger the  $+\Psi_{+q-coil}$ , the more the magnetic shielding effect on the PM-flux vector works and the magnetic flux becomes a flow of magnetic flux that forms leakage magnetic flux in the iron core magnetic flux path.

Next, it is considered using vector distribution simulated FE-analysis and vector diagram to push forward an analysis about variable magnetic flux function of the proposed motor. First, consider the magnet torque characteristics of the benchmark in Fig. 8 (c). When the armature magnetomotive force is high, with respect to the theoretical characteristic of the magnet torque of the ideal  $\cos\beta$  function, the magnet torque near the current phase  $\beta = 0$  deg. Especially when the current phase is 0 deg, the magnetic shielding effect occurs due to the influence of the  $q$ -axis armature reaction  $L_q i_q$  orthogonal to the PM-flux  $\Psi_m$  as shown in Fig. 10, the  $d$ -axis magnetic resistance increases and the PM-flux  $\Psi_m$  becomes the demagnetization action. As a result, it changes from the dotted line vector diagram (without considering reduction of  $\Psi_m$ ) to the solid line vector diagram (with consideration for decreasing  $\Psi_m$ ) in Fig. 10 (b). Here, although the  $L_q i_q$  magnetic path exists also on the inner diameter side of the rotor, it contributes less to the reduction of  $\Psi_m$ , it is not indicated by a black line arrow. On the other hand, when the current phase is other than 0 deg, for example, in the case of -30 deg shown in Fig. 11, the flux intensifying effect differs between the

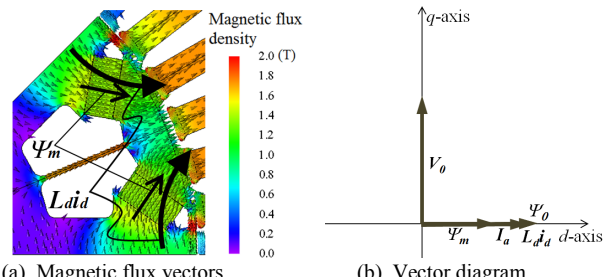


Fig. 12. Magnetic flux vectors and vector diagram under high-load and current phase -90 deg. (Benchmark).

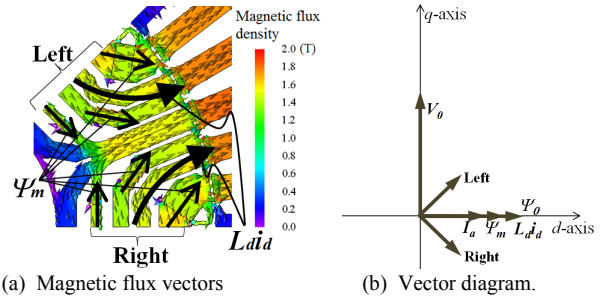


Fig. 13. Magnetic flux vectors and vector diagram under high-load and current phase -90 deg. (Proposed).

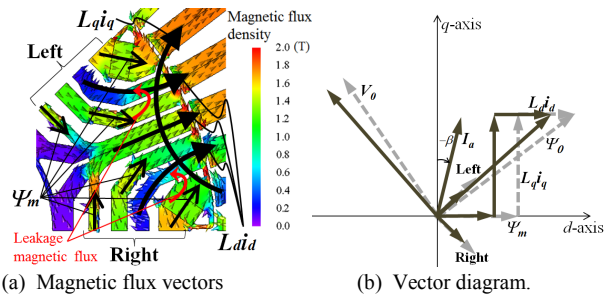


Fig. 14. Magnetic flux vectors and vector diagram under high-load and current phase -60 deg. (Proposed).

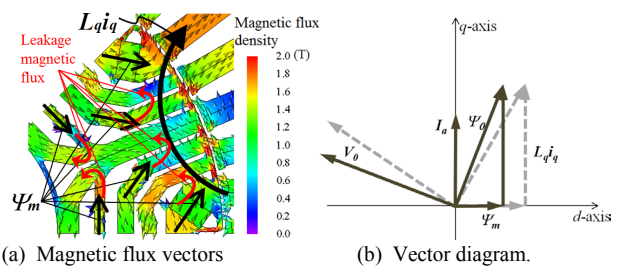
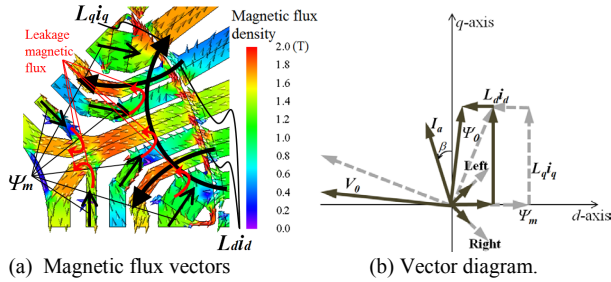
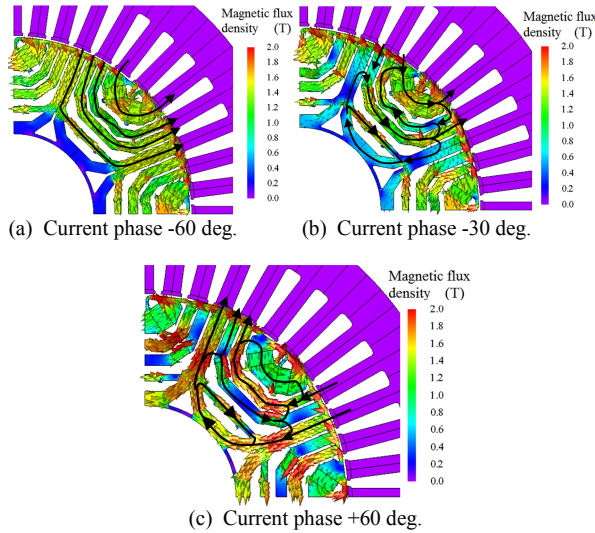


Fig. 15. Magnetic flux vectors and vector diagram under high-load and current phase 0 deg. (Proposed).

right side and the left side of the magnet arranged in the V-shape in the magnetic pole. As a result, a phase shift of the PM-flux vector occurs with respect to the  $d$ -axis in the case of the current phase of -90 deg in Fig. 12. Here, the phase of  $\Psi_m$  is an image diagram. The  $q$ -axis armature reaction  $L_q i_q$  is orthogonal to  $\Psi_m$  and the magnetic resistance of the  $d$ -axis increases to act as a demagnetization action. In addition, the  $d$ -axis armature reaction  $L_d i_d$  in the same direction (flux intensifying direction) as the PM flux vector also orthogonally acts so



(a) Magnetic flux vectors (Current phase: +30 deg).  
 Fig. 16. Magnetic flux vectors and vector diagram under high-load and current phase +30 deg. (Proposed).



(c) Current phase +60 deg.  
 Fig. 17. PM-flux vectors with respect to current phase.

that the flux intensifying of the right magnet becomes strong in the case of CCW rotation. Thus, this is due to interference of the magnetic paths between the  $dq$ -axes, and since this influence is not taken into account in the mathematical model of the theoretical  $dq$ -axis, there is a difference between the magnet torque of the theoretical  $\cos\beta$ -function of the mathematical model and the actual measurement value.

Next, consider the magnet torque of the proposed motor. Figure 13 to 16 show the magnetic flux vector distribution and the  $dq$ -axis vector diagram when the current phase is changed. The vector diagram of each figure is drawn in the image diagram. Comparing the figures, as the current phase advances from -90 deg (flux intensifying) to + $q$ -axis direction, the flux intensifying effect due to the + $d$ -axis armature magnetic flux decreases and the leakage magnetic flux increases due to the magnetic shielding effect by the  $q$ -axis armature magnetic flux, therefore the amount of magnetic flux linking the armature winding decreases. As a result, in the vector diagram of each figure (b), a dotted line vector (without considering the leakage magnetic flux) is changed to a solid line vector (with leakage magnetic flux). On the other hand, Fig. 16 shows a diagram showing only the DC magnetic flux in the rotor by using the harmonic analysis function of the electromagnetic field analysis software (JMAG-Designer ver.15). As shown in Fig. 17 (a) and (b), as the current phase  $\beta$  advances from + $d$ -axis to + $q$ -axis direction, the leakage

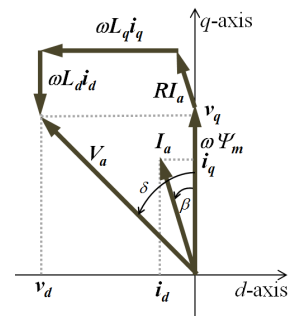


Fig. 18. Vector diagram of PM-motor.

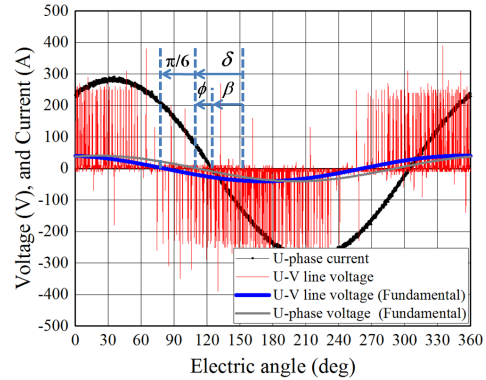


Fig. 19. Measured voltage and current.

magnetic flux increases as indicated by an arrow through an iron core magnetic flux path provided between the PM-flux paths. On the other hand, as shown in Fig. 17 (c), according to the current phase  $\beta$  advancing from the + $q$ -axis to the - $d$ -axis direction (flux weakening region), as explained in Fig. 2 (e), - $d$ -axis armature magnetic flux forms a closed magnetic flux path between the iron core magnetic flux path and the stator via an air-gap, the leaking PM-flux will not be short-circuited within the rotor and will be linked to the armature winding, resulting in an increase in armature flux linkage. Considering the actual driving, basically it is driven at the MTPA point, so it is driven in the flux intensifying region of the forward salient pole type proposed motor, and it can be inferred that the influence of this driving characteristic on the performance is small.

**B. dq-axis Voltage Ellipse**

Next, the drive performance is considered by visualizing the trajectory of the  $dq$ -axis voltage ellipse. As shown in the vector diagram of Fig. 18, if the value of the voltage phase  $\delta$  is known,  $v_d$  and  $v_q$  can be obtained from Eq. (1) [21].

$$v_d = -V_1 \sin \delta, \quad v_q = V_1 \cos \delta \quad (1)$$

Voltage phase  $\delta$  is measured by operating the test motor at a constant speed with arbitrary armature magnetomotive force and current phase, measuring UV-line voltage and U-phase current by an oscilloscope, and deriving the fundamental wave with an FFT analyzer. As an example, Fig. 19 shows the measured UV-line voltage and U-phase current, the UV-line voltage fundamental wave and the U-phase voltage fundamental wave calculated by postprocessing at a rotation speed of 500 r/min, the armature magnetomotive force of 600  $A_{rms}T$ ,

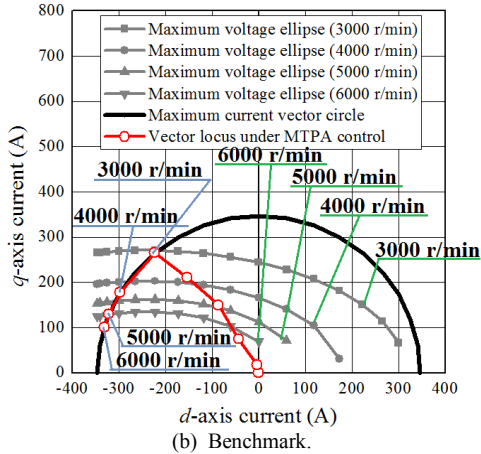
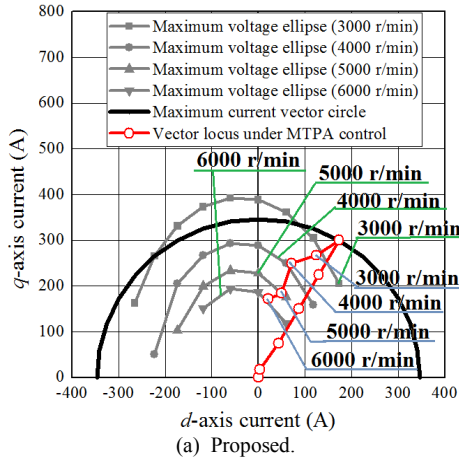


Fig. 20. Vector locus under MTPA control.

and the current phase of +30 deg. From this figure, the voltage phase  $\delta$  is obtained.

Figure 20 shows the current-limited circle, the  $dq$ -axis voltage ellipse, and the current vector trajectory in MTPA control, where  $v_d$  and  $v_q$  are obtained from actually measured voltage phase and current phase information [21]. As shown in this figure, the proposed motor has forward saliency, so that  $v_q > v_d$ , and the  $i_q$ -axis becomes the long axis radius of the voltage ellipse. As a result, when it comes to voltage limitation, it can not be driven within the voltage threshold unless it is a current vector trajectory that reduces the armature current norm rather than the current phase advance. On the other hand, since the benchmark is a reverse salient pole, the  $i_d$ -axis becomes the long axis radius of the voltage ellipse. As a result, when it comes to voltage limitation, the current norm is not changed and the current phase is advanced to drive within the voltage threshold. From these results, it is clear from the current vector trajectory that the leakage magnetic flux effect due to the current phase advance of the proposed motor can not be utilized to improve the drive characteristics.

### C. Efficiency Map

Figure 21 shows the motor efficiency map in motoring. From the figure, the motor efficiency is significantly lower than the benchmark. In particular, the peak efficiency was about 4 % lower. From the measurement result of the torque characteristic, it was possible to

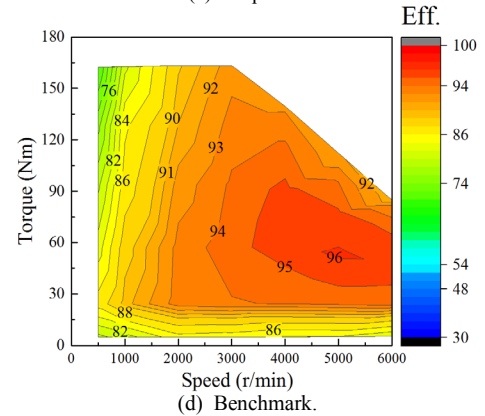
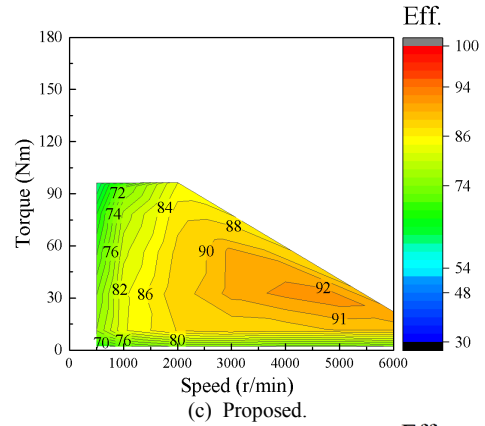


Fig. 21. Efficiency maps in motoring under 750  $A_{rms}$  T limitation. (Limited under 70 %-load.)

demonstrate the variable flux function, but the difference in performance from the magnet type reverse salient pole motor due to the essential problem of the magnet type forward salient pole motor structure rather than the performance improvement effect by the variable magnetic flux was revealed. In the case of the magnet type forward salient pole structure, as mentioned in the previous section, the low torque density due to the fundamental magnetic circuit by the non-interference design of the  $dq$ -axis magnetic path and the current norm adjustment type variable speed drive due to the major axis radius of the voltage ellipse on the  $i_q$ -axis appears remarkably in efficiency drops.

### V. CONCLUSION

In this paper, applying the feature of a consequent pole structure, the study was presented on a motor featuring enhanced salient pole ratio, variable leakage magnetic flux function, and flux intensifying by  $d$ -axis armature magnetic flux by arranging the PM-flux path and the iron core magnetic flux path alternately. As a result of the actual machine evaluation, the variable magnetic flux effect described above could be demonstrated. By visualizing the vector locus, it was also clarified that the variable magnetic flux effect due to the current phase advance was not able to contribute to performance improvement. It is because that the feature of the variable speed drive characteristic by the current-norm adjustment type drive of the forward salient pole motor. As a result of this study, it was clarified that in the case of realizing

passive variable magnetic flux due to variable leakage magnetic flux characteristics in the magnet type, it is not possible to fully utilize the variable magnetic flux effect for improving drive characteristics with forward salient pole type.

According to the results of this study, it is preferable to design the variable leakage magnetic flux motor with a reverse salient pole structure with a low salient pole ratio and designed, so that the magnet torque can be utilized to the utmost. And it can be considered that the magnetic circuit design in which the leakage magnetic flux increases with the  $d$ -axis armature magnetic flux above the nominal speed is more suitable from the viewpoint of extending the adjustable speed drive characteristic. The future work is to investigate the magnetic circuit of the variable leakage magnetic flux motor with the magnetic circuit design which can be utilized to the utmost magnet torque and increase leakage magnetic flux in proportion to negative  $d$ -axis armature magnetic flux increase.

## REFERENCES

- [1] <https://www.tesla.com/jp/blog/induction-versus-dc-brushless-motors>
- [2] Y. Sato, S. Ishikawa, T. Okubo, M. Abe, and K. Tamai: "Development of High Response Motor and Inverter System for the Nissan LEAF Electric Vehicle", *SAE Technical Paper*, No. 2011-01-0350 (2011).
- [3] K. Handa, H. Yoshida: "Development of Next-Generation Electric Vehicle i-MiEV", *Mitsubishi Motors Technical Review*, No. 9, pp. 65-69 (2007) (in Japanese).
- [4] F. Momen, K. Rahman, Y. Son, and P. Savagian: "Electrical Propulsion System Design of Chevrolet Bolt Battery Electric Vehicle", *IEEE Energy Conversion Congress and Expo (ECCE)* (2016).
- [5] Ostovic, V.: "Memory Motors", *IEEE Industry Applications Magazine*, vol. 9, pp.52-61 (2003).
- [6] Ostovic, V. : "Memory Motors – a New Class of Controllable Flux PM Machines for a True Wide Speed Operation", *Proc. of IEEE Industry Applications Society Conference*, 2001, vol. 4, pp.2577-2584 (2001).
- [7] K. Sakai, K. Yuki, Y. Hashiba, N. Takahashi, K. Yasui, and L. Kovudhikulrungsri: "Principle and Basic Characteristics of Variable Magnetic-Force Memory Motors", *IEEJ Trans. on IA.*, vol. 131, No. 1 pp.53-60 (2011) (in Japanese).
- [8] T. Kato, N. Limsuwan, C. Y. Yu, K. Akatsu, and R. D. Lorenz: "Rare Earth Reduction Using a Novel Variable Magnetomotive Force, Flux Intensified IPM Machine", *IEEE Trans. on IA.*, vol. 50, No. 3, pp.1748-1756 (May/June, 2016).
- [9] T. Nonaka, S. Oga, and M. Ohto: "Consideration about the Drive of Variable Magnetic Flux Motor", *IEEJ Trans. on IA.*, vol. 135, No. 5, pp. 451-456 (2015) (in Japanese).
- [10] T. Mizuno, K. Nagayama, T. Ashikaga, and T. Kobayashi: "Basic Principles and Characteristics of Hybrid Excitation Type Synchronous Machine", *IEEJ Trans. on IA.*, vol. 115, No. 11, pp.1402-1411 (1995) (in Japanese).
- [11] J. A. Tapia, F. Leonardi, and T. A. Lipo: "Consequent-Pole Permanent-Magnet Machine with Extended Field-Weakening Capability", *IEEE Trans. on IA.*, vol. 39, No. 6, pp.1704-1709 (2003).
- [12] M. Namba, K. Hiramoto, and H. Nakai: "Novel Variable-Field Motor with a Three-Dimensional Magnetic Circuit", *IEEJ Trans. on IA.*, vol. 135, No. 11, pp.1085-1090 (2015) (in Japanese).
- [13] T. Ogawa, T. Takahashi, M. Takemoto, H. Arita, A. Daikoku, and S. Ogasawara: "The Consequent-Pole Type Ferrite Magnet Axial Gap Motor with Field Winding for Traction Motor Used in EV", *SAEJ Proc. of EVTeC & APE Japan 2016*, No. 20169094 (2016).
- [14] T. Kato, M. Minowa, H. Hijikata, and K. Akatsu: "High Efficiency IPMSM Effectively Utilizing Variable Leakage Flux Characteristics", *IEEJ JIASC 2014*, No. 3-13, pp. 139-142 (2014) (in Japanese).
- [15] T. Kato, and K. Akatsu: "Magnet Operating Point Characteristics of Variable Leakage Flux Interior Permanent Magnet Motor", *IEEJ JIASC 2015*, No. 3-1, pp. 65-70 (2015) (in Japanese).
- [16] A. Athavale, T. Fukushige, T. Kato, C.Y. Yu, and R. D. Lorenz: "Variable Leakage Flux (VLF) IPMSMs for Reduced Losses over a Driving Cycle while Maintaining the Feasibility of High Frequency Injection-Based Rotor Position Self-Sensing", *IEEE Energy Conversion Congress and Exposition (ECCE)*, (2014).
- [17] M. Minowa, H. Hijikata, K. Akatsu, and T. Kato: "Variable Leakage Flux Interior Permanent Magnet Synchronous Machine for Improving Efficiency on Duty Cycle", *International Power Electronics Conference (IPEC-Hiroshima 2014 –ECCE ASIA)*.
- [18] I. Urquhart, D. Tanaka, R. Owen, Z. Q. Zhu, J. B. Wang, and D. A. Stone: "Mechanically Actuated Variable Flux IPMSM for EV and HEV Applications", *Proc. of EVS27 International Battery, Hybrid and Fuel Cell Vehicle Symposium 2013*, pp. 0684-0695 (2013).
- [19] M. Aoyama, K. Nakajima, and T. Noguchi: "Preliminary Study of Flux Intensifying PM Motor with Variable Leakage Magnetic Flux Technique", *IEEJ Annual Meeting*, No. 5-001, pp. 1-2 (2017) (in Japanese).
- [20] M. Aoyama, K. Nakajima, and T. Noguchi: "Driving Performance of Flux Intensifying PM Motor with Variable Leakage Magnetic Flux Technique", *IEEJ JIASC*, No. 3-42, (2017) (in Japanese).
- [21] M. Morimoto, Y. Takeda, and T. Hirasaka: "Parameter Measurement of PM Motor in  $dq$  Equivalent Circuit", *IEEJ Trans. on IA.*, vol. 113, No. 11, pp.1330-1331 (1993) (in Japanese).